J. Cent. South Univ. (2016) 23: 3312−3321
DOI: 10.1007/s11771-016-3397-1

Springer

Model test to investigate failure mechanism and loading characteristics of shallow-bias tunnels with small clear distance

LEI Ming-feng(雷明锋)[1, 2], LIN Da-yong(林大涌)[1], YANG Wei-chao(杨伟超)[1], SHI Cheng-hua(施成华)[1], PENG Li-min(彭立敏)[1], HUANG Juan(黄娟)[1]

1. School of Civil Engineering, Central South University, Changsha 410075, China;
2. China Construction Fifth Engineering Division Corp., Ltd., Changsha 410004, China

Abstract: Based on the similarity theory, a tunnel excavation simulation testing system under typical unsymmetrical loading conditions was established. Using this system, the failure mechanism of surrounding rock of shallow-bias tunnels with small clear distance was analyzed along with the load characteristics. The results show that: 1) The failure process of surrounding rock of shallow-bias tunnels with small clear distance consists of structural and stratum deformation induced by tunnel excavation; Micro-fracture surfaces are formed in the tunnel surrounding rock and extend deep into the rock mass in a larger density; Tensile cracking occurs in shallow position on the deep-buried side, with shear slip in deep rock mass. In the meantime, rapid deformation and slip take place on the shallow-buried side until the surrounding rocks totally collapse. The production and development of micro-fracture surfaces in the tunnel surrounding rock and tensile cracking in the shallow position on the deep-buried side represent the key stages of failure. 2) The final failure mode is featured by an inverted conical fracture with tunnel arch as its top and the slope at tunnel entrance slope as its bottom. The range of failure on the deep-buried side is significantly larger than that on the shallow-buried side. Such difference becomes more prominent with the increasing bias angle. What distinguishes it from the "linear fracture surface" model is that the model proposed has a larger fracture angle on the two sides. Moreover, the bottom of the fracture is located at the springing line of tunnel arch. 3) The total vertical load increases with bias angle. Compared with the existing methods, the unsymmetrical loading effect in measurement is more prominent. At last, countermeasures are proposed according to the analysis results: during engineering process, 1) The surrounding rock mass on the deep-buried side should be reinforced apart from the tunnel surrounding rock for shallow-buried tunnels with small clear distance; moreover, the scope of consolidation should go beyond the midline of tunnel (along the direction of the top of slope) by 4 excavation spans of single tunnel. 2) It is necessary to modify the load value of shallow-bias tunnels with small clear distance.

Key words: shallow-bias; tunnels with small spacing; failure mechanism; loading characteristics; model test

1 Introduction

Small clear distance tunnels have the advantages of less space occupation, easy route development and acceptable construction cost, and therefore have been found wide applications in transport infrastructures [1]. Compared with conventional separated double track tunnel, small clear distance tunnels usually present a more complex stress pattern [2]. Those with a shallow burial depth are more easily affected by geological conditions and terrain-induced unsymmetrical loading. Construction of such tunnels may incur severe accidents because of high construction difficulty and risk.

To address this problem, a 10t of research has been carried out to optimize the method for calculating the surrounding rock pressure for small clear distance tunnels [3−5], investigate the mechanical behaviors during construction [6−11], and develop reasonable construction sequence [12] and monitoring & measurement techniques [13−14]. For example, XIAO [15] established the calculation model for surrounding rock pressure of small clear distance tunnels in 2004 based on limit equilibrium theory of blocks. The calculation results of surrounding rock pressure based on the assumption of “broken-line fracture surface” and “linear fracture surface” were compared, and the applicability of the calculation model was discussed. Later, SHU et al [16] established the slip fracture model of surrounding rock for shallow-buried tunnels with small clear distance combining with the real stress pattern under unsymmetrical loading. They also derived

Foundation item: Project(51508575) supported by the National Natural Science Foundation of China; Project (2011CB013802) supported by the National Basic Research Program of China; Projects(2014M560652, 2016T90764) supported by the China Postdoctoral Science Foundation; Project(2015RS4006) supported by the Innovative Talents of Science and Technology Plan of Hunan Province, China
Received date: 2015−06−03; **Accepted date:** 2015−11−19
Corresponding author: YANG Wei-chao, Lecturer, PhD; Tel: +86−13787232438; E-mail: 124520238@qq.com

the calculation formulas for surrounding rock pressure. With the consideration of the interaction between caverns, YANG et al [17] obtained the upper bound solution of surrounding rock pressure for three shallow-bias track tunnels with small clear distance.

These research achievements contribute to the progress of construction techniques of small clear distance tunnels. However, the existing researches on small clear distance tunnels have their shortcomings when applied to practice [18]. For example, the above researches on surrounding rock pressure calculation [15−17] are mostly based on the assumption of "linear fracture surfaces", which is a great departure from real situation. Insufficient understanding on the failure mechanism of surrounding rock of shallow-bias tunnels with small clear distance is the main reason for the inaccuracy in the construction of failure mode and the assumption of loading characteristics. We performed indoor experiments to investigate the failure mechanism of surrounding rock mass of shallow-bias tunnels with small clear distance along with the load characteristics.

2 Experimental design

2.1 Similar relations and similar materials

The geometry similarity ratio between the real tunnel and the model was set as 20:1, and the bulk density similarity ratio as 2:1. Then using similarity theory, the similarity ratios of other physical quantities were calculated, as shown in Table 1. The process of derivation was referred from Refs. [19−20].

Table 1 Similarity ratios of model test parameters

Quantity	Similarity ratio
Geometry	20
Volume-weight	2
Elastic modulus	40
Poison ratio	1
Cohesion	1
Stress	40
Rock pressure	40

The objective of the present research was to understand the failure mechanism and load characteristics of surrounding rock of shallow-bias tunnels with small clear distance. However, the mechanical properties of supporting structure were disregarded. Therefore, only similarity of surrounding rock materials was considered, while the supporting structure was made of 1.2 mm thick iron sheet (see Fig. 1).

The stratum conditions of grade-Ⅴ surrounding rock of one expressway tunnel in China were first analyzed. A large number of compressive strength tests were carried out using cubic blocks to determine similar materials and their proportion as clay to slag to river sand=1:1:2. The corresponding mechanical parameters are shown in Table 2 [19−20].

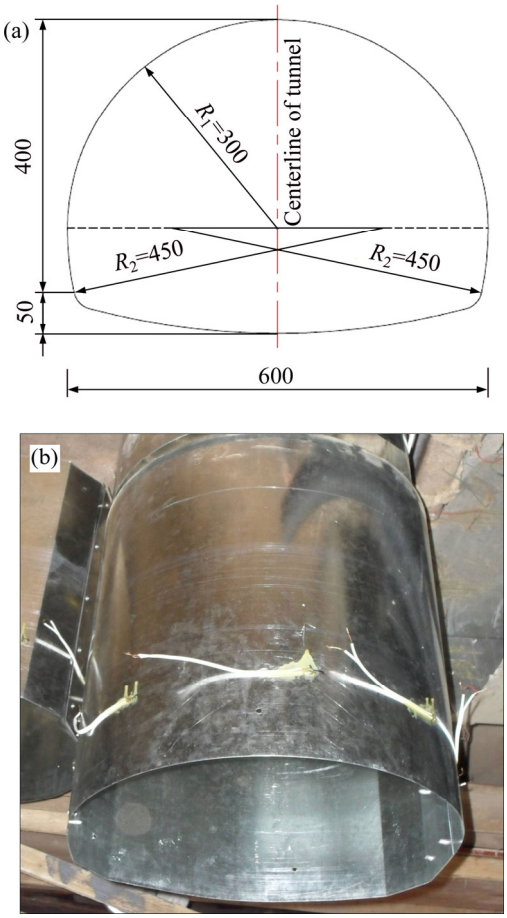

Fig. 1 Model of tunnel lining structure (Unit: mm): (a) Model dimension; (b) Model entity

2.2 Working conditions and tests

The test was carried out in a customized model box (Fig. 2). Three typical angles of terrain-induced unsymmetrical loading were considered, namely, 15°, 30° and 45°. Special pressure cells were used for testing the surrounding rock pressure. The arrangement of testing cross section and testing points are shown in Fig. 3. The failure pattern of surrounding rock was observed.

Benching tunneling method was employed for excavation considering operability and representative-ness of the excavation regime. The excavation sequence was as follows: the right tunnel (deep-buried side) was first excavated, and advanced by 3 cycles than the left tunnel (shallow-buried side), with 0.2 m for each cycle; the upper bench advanced by 1.0 m than the lower bench.

As shown in Fig. 4, the shaded blocks indicate "excavation".

Table 2 Parameters of model and prototype materials

Item	Volume-weight/(kN·m^{-3})	Elastic modulus/GPa	Poisson ratio	Internal friction angle/(°)	Cohesion/kPa
Prototype	19.00	1	0.45	18	30
Model	9.53	0.025	0.45	18	30

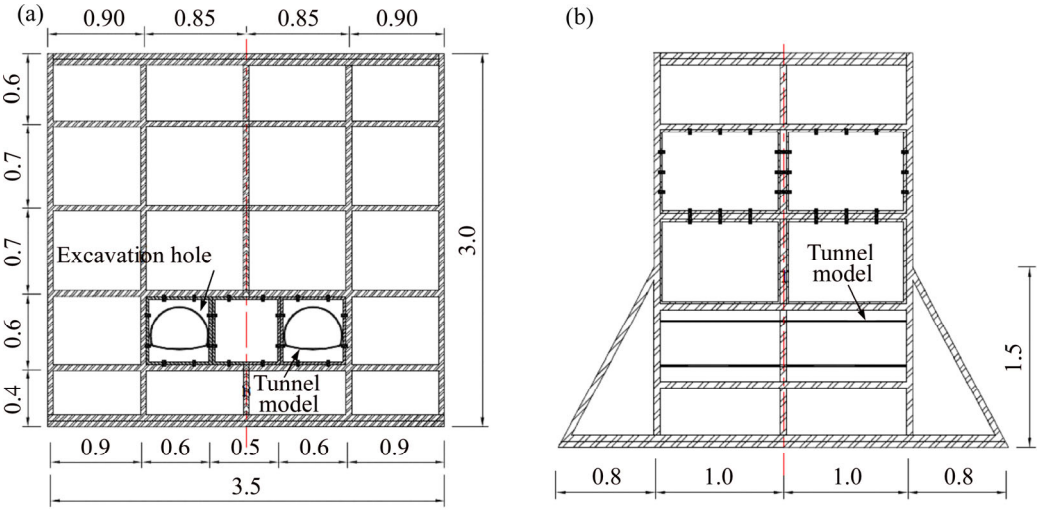

Fig. 2 Model test chamber (Unit: m): (a) Front view; (b) Side view; (c) Real picture

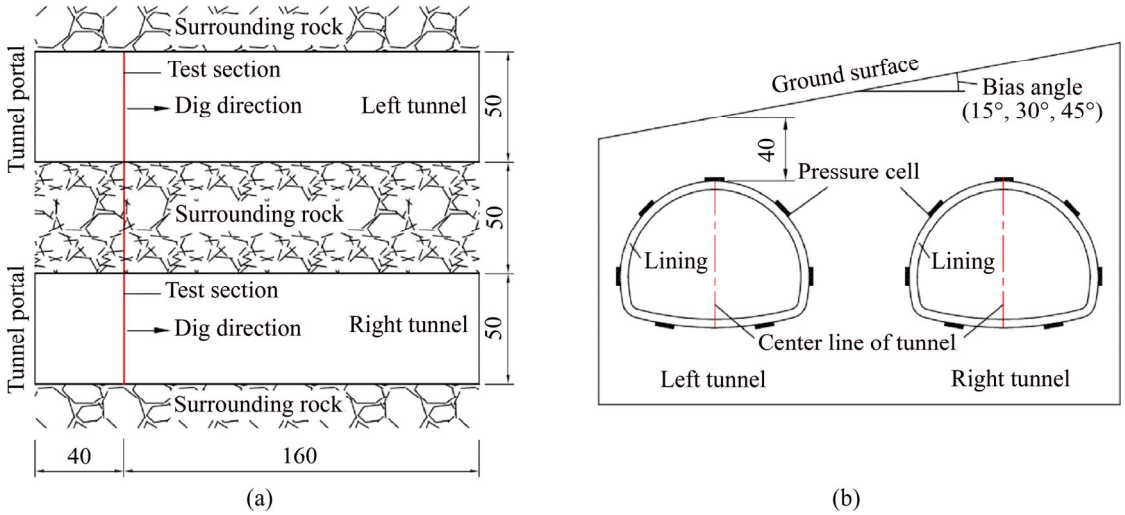

Fig. 3 Locations of test section and measuring points (Unit: cm): (a) Test section; (b) Measuring points

2.3 Experimental procedures

1) Model box shown in Fig. 2 was fabricated, with the inner surface on four sides covered with plastic films. A layer of oil was applied to reduce the friction between the model box and the surrounding rock.

2) The dose of each component was calculated

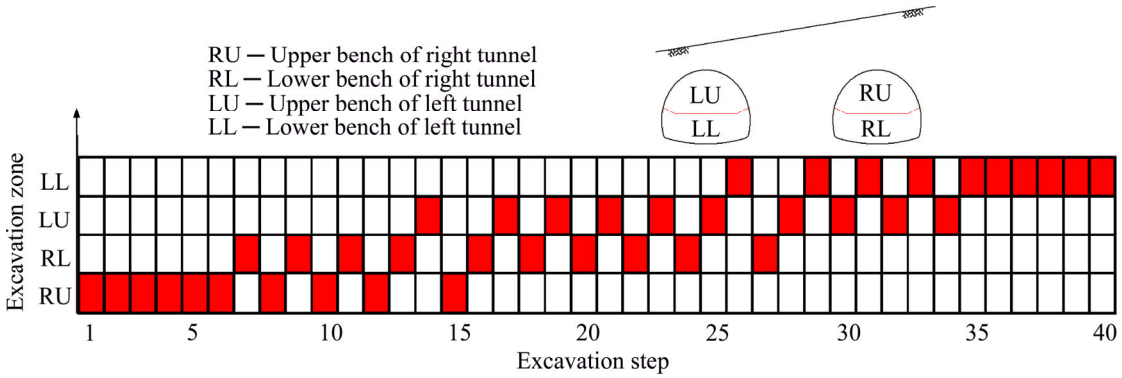

Fig. 4 Drilling footage of model test

according to the similarity ratio. The raw materials were weighed, loaded into the mixer and mixed well. The tunnel model was prepared by scale (Fig. 1).

3) After installation, similar materials were filled into the bottom of the model box until reaching 0.5 m above the bottom. Compaction was performed to avoid large settlement and model failure while ensuring the pressure of overlying earth on the tunnel model.

4) The lining model was installed to the predetermined position. The earth inside the lining was made into "blocks" with similar shape as excavation step. The blocks were wrapped in plastic films and applied with oil on the outside. Then, the blocks were placed inside the tunnel lining to simulate unexcavated state.

5) "Earth blocks" were uniformly filled on the two sides of lining model to obtain unsymmetrical loading model under various working conditions. According to the burial depth of shallow-buried section in real project and using similarity theory, the minimum thickness of overlying earth for surrounding rock on top of the tunnel was determined as 0.4 m. The pressure cells were successively buried in the predetermined positions, as shown in Fig. 3(b).

6) After placement for 48 h, the initial values of each pressure cell were read.

7) Corresponding blocks were withdrawn from the lining model according to excavation regime. For each excavation step, the pressure values were read.

8) When the excavation and test is complete according to the preset working procedure, the external load is applied to the ground surface, and the external load gradually increases until the model structure is damaged. During this process, the failure characteristics of surrounding rock were recorded in detail.

3 Failure mechanism

3.1 Failure process

Before excavation, the original strata maintain stress equilibrium. As excavation proceeds, the original stress equilibrium is disrupted in the surrounding rock. The stress pattern of the strata constantly changes during excavation, showing a cycle of disequilibrium−adjustment−equilibrium regained. When the tunnel or surrounding rock cannot provide sufficient supporting strength, the tunnel or surrounding rock will fail. The process of progressive failure can be represented as follows:

1) Before excavation, the strata where the tunnel is located are in equilibrium (Fig. 5(a)).

2) As the excavation proceeds, stress is produced and released, leading to gradual increase of stress on the tunnel. Deformation related to unsymmetrical loading occurs and is then propagated to surface, resulting in subsidence groove (Fig. 5(b)).

3) When excavation is finished, overloading is applied to ground surface. Tunnel deformation is intensified; the deformation of tunnel on the deep-buried side is larger than that on the shallow-buried side; the left haunch of tunnel on the deep-buried side has the largest displacement, followed by right foot on the shallow-buried side (Fig. 5(c)).

4) Several fracture surfaces appear in the surrounding rock, and the cracks on the deep-buried side show an increasing density. The fracture surfaces continue to increase and expand until they are interconnected (Fig. 5(d)).

5) As the deformation of the surrounding rock continues to develop, tensile cracking occurs in the strata of shallow position on deep-buried side. The rock mass over the tunnel is the first to undergo rapid slip, and the surrounding rock on the shallow-buried side comes next. The two collapse almost at the same time, forming the collapsing body (Fig. 5(e)).

As seen from the above analysis, the development of failure of shallow-bias tunnels with small clear distance can be summarized as follows: deformation of tunnel and strata → deformation propagating to ground surface to lead to subsidence groove and micro-fracture surfaces in the periphery of tunnel → fracture surfaces

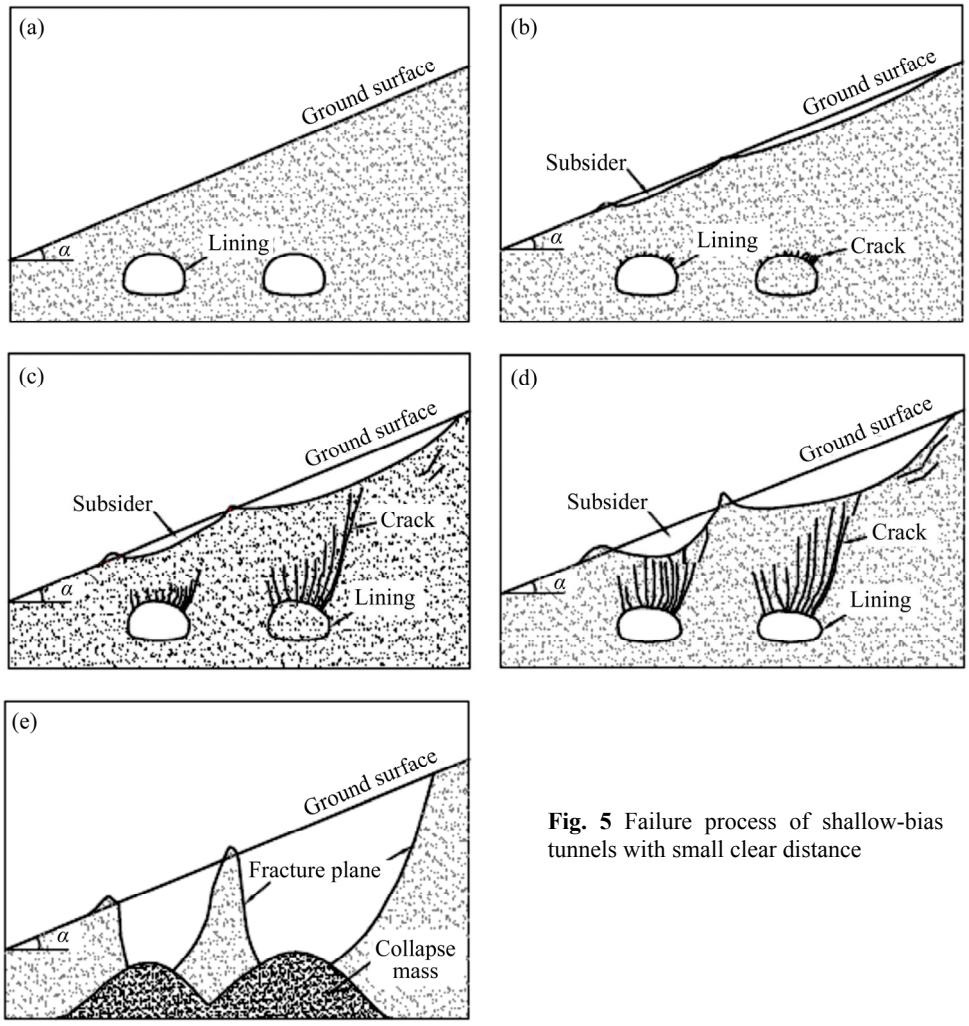

Fig. 5 Failure process of shallow-bias tunnels with small clear distance

extending deep into the surrounding rock in a larger density → tensile cracking in shallow position on deep-buried side and shear slip in deep layer → rapid deformation and slip on shallow-buried side → collapse. Further analysis revealed that the vulnerable site of shallow-buried small clear distance tunnels with unsymmetrical loading is the periphery of the tunnel and the strata in shallow position on deep-buried side. The deformation of surrounding rock and the appearance of micro-fracture surfaces provide initial conditions for failure of the surrounding rock. Tensile cracking of the shallow position on deep-buried side aggravates or directly leads to the overall failure of surrounding rock.

During project design and construction, these two vulnerable sites should be reinforced and closely monitored. For example, grouting reinforcement should be performed in the tunnel surrounding rock to reduce deformation of tunnel and surrounding rock and to avoid or delay the appearance of micro-fracture surfaces. For reinforcement of surrounding rock on the deep-buried side, small pipe (anchor bolt) grouting is preferred to reduce the formation of tensile fracture surfaces on shallow ground or inhibit their development.

3.2 Failure mode

The failure model of surrounding rock of shallow-bias tunnels with small clear distance was obtained from the morphology of fracture surfaces after failure, as shown in Fig. 6, where D is the excavation span of a single tunnel.

It can be known from analysis as follows.

1) The fracture mode of shallow-bias tunnels with small clear distance is dominated by an inverted conical fracture with tunnel arch as top and the slope at tunnel entrance as its bottom. The range of surface fracture on the shallow-buried side is about (1.5−2)D, and that on the deep-buried side is about (2−5)D, which is obviously larger than the former. As the angle of unsymmetrical loading increases, the range of fracture increases as well; the increasing trend on the deep-buried side is especially prominent. When this angle is 45°, the range of fracture of surrounding rock on the deep-buried side will reach 5D.

Combining with the above analysis, we suggest that the surrounding rock mass on the deep-buried side should be also reinforced apart from the surrounding rock in the periphery of shallow-buried small clear

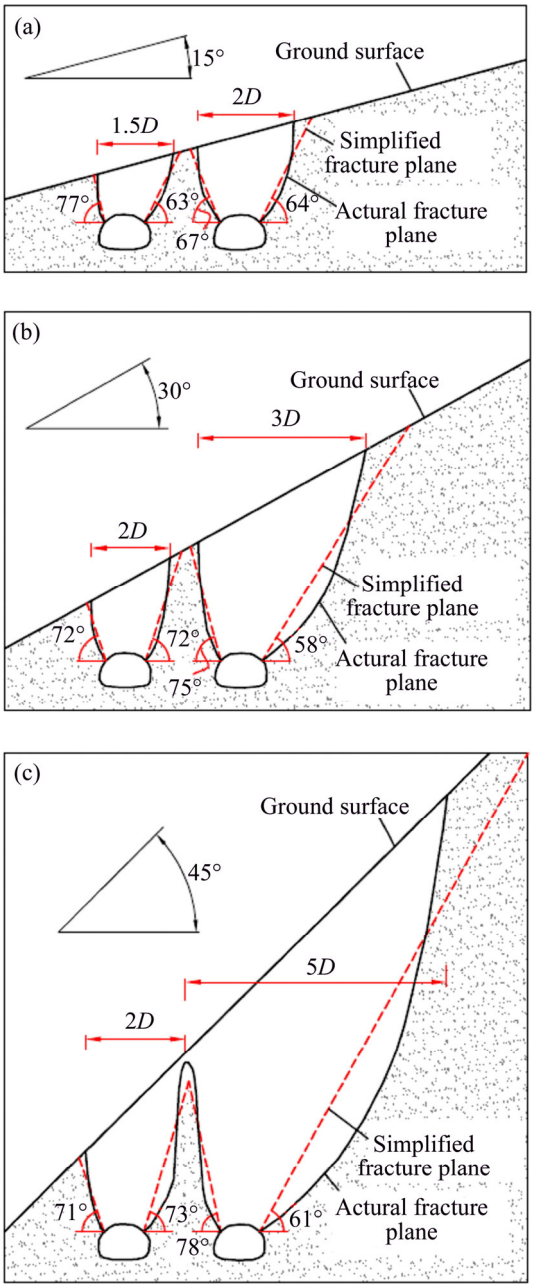

Fig. 6 Failure modes of tunnels at different bias angles: (a) 15°; (b) 30°; (c) 45°

distance tunnels. Moreover, the scope of reinforcement should go beyond the midline of the tunnel by 4*D* (in the direction of the top of slope).

2) The morphology of fracture surfaces over the sidelines of the deep-buried side is similar to that of a single tunnel [19−20]. The fracture angle on the shallow-buried side is larger than that on the deep-buried side. The average fracture angles on the deep-buried and shallow-buried sides under experimental working conditions are about 65° and 73°, respectively (Fig. 7).

However, the fracture angle on the shallow-buried side is smaller than that on the deep-buried side for middle rock pillar. Generally, the obtained fracture angle

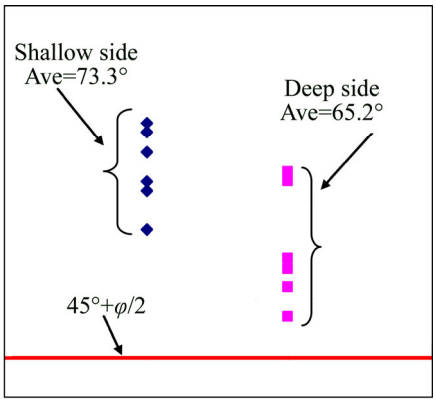

Fig. 7 Distribution characteristics of rupture angle of shallow-bias tunnels with small clear distance

of the surrounding rock is larger than what is conventionally conceived (45°+φ/2), but more similar to the value calculated in Ref. [16].

3) As the angle of unsymmetrical loading, the intersection between the fracture lines on the two sides of middle rock pillar begins to move downwards until reaching the ground surface under the experimental working conditions.

Thus, the failure mode of shallow-bias tunnels with small clear distance can be derived, as shown in Fig. 8. Compared with "linear fracture surface" model described in Ref. [16], the model proposed has larger fracture angles on the two sides and smaller scope of fracture, and the fracture angles on the two sides of the middle rock pillar are smaller. The bottom of the fracture is located at the springing line of tunnel arch, rather than the foot of side wall.

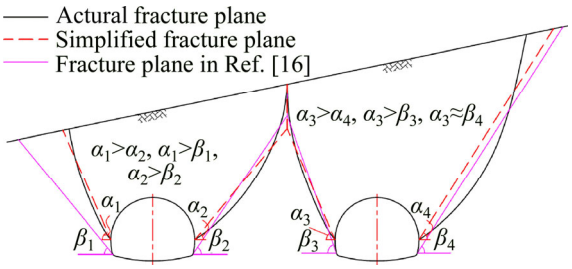

Fig. 8 Failure mode of shallow-bias tunnels with small clear distance

4 Load characteristics

The final pressure values of surrounding rock measured after excavation according to the predetermined regime (see Fig. 4) were processed based on the assumption of linear distribution. Then, the surrounding rock pressure of the supporting structure was obtained under different angles of unsymmetrical loading, as shown in Fig. 9. To verify the reliability of the experimental results, the calculations by Ref. [16]

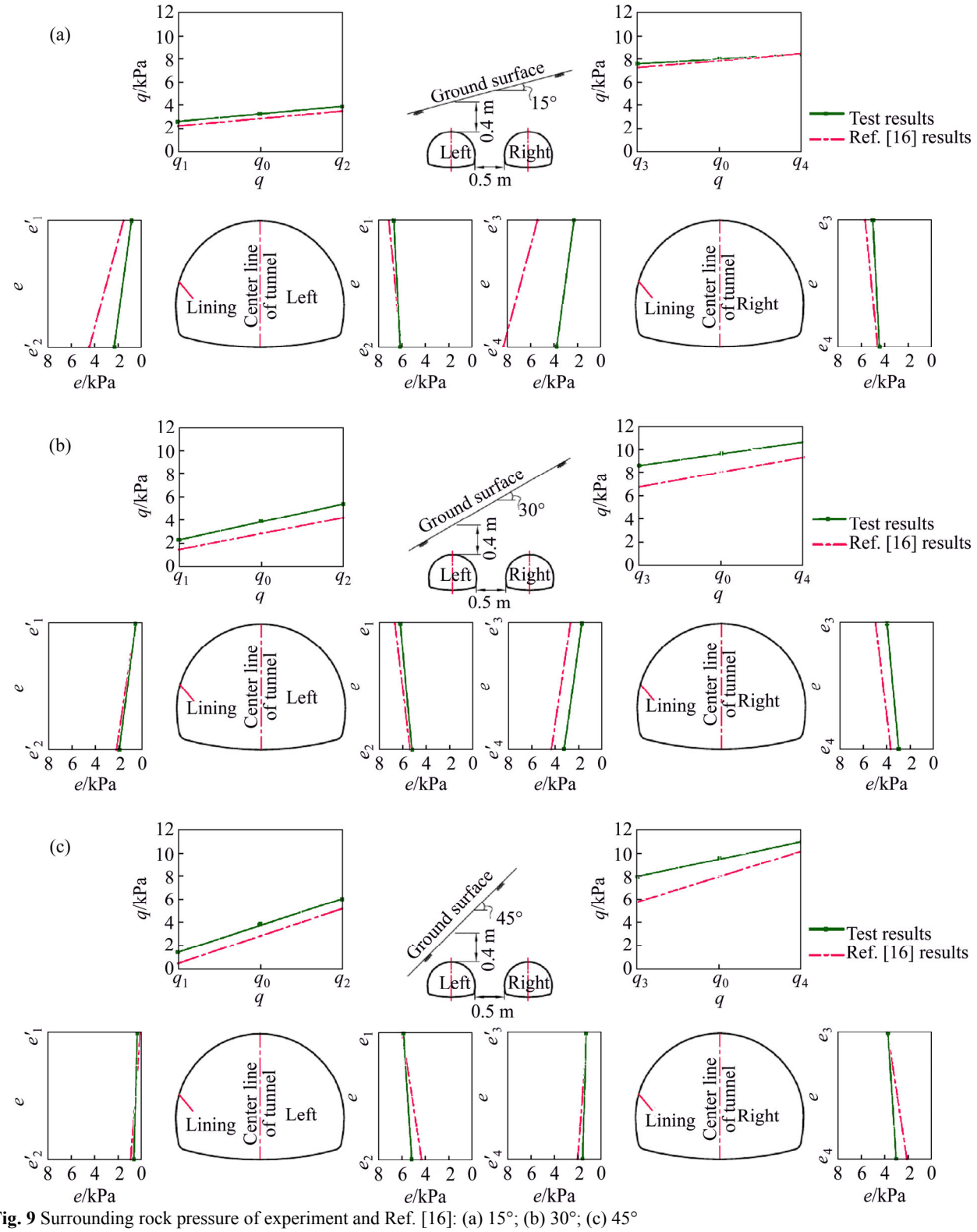

Fig. 9 Surrounding rock pressure of experiment and Ref. [16]: (a) 15°; (b) 30°; (c) 45°

under similar working conditions were included in Fig. 9.

4.1 General distribution characteristics

1) In general (Fig. 9), both vertical loads and horizontal loads of the deep-buried side (right) are larger than those of the shallow-buried side (left), indicating obvious unsymmetrical loading effect. This is consistent with the existing research findings [16].

2) Comparison is made with the calculations in Ref. [16], and similarity in overall distribution pattern of the two is noted. The load results are very similar on the shallow-buried side. When bias angle is small on the deep-buried side (i.e. α=15°), the vertical loads are very

similar. As the bias angle increases, experimental result in the present study is larger than the calculation in Ref. [16]. When this angle is 45°, the total vertical load is about 1.22 times that of the calculation in Ref. [16]. Horizontal load shows the opposite variation trend. When this angle is 15°, the total horizontal load in the present study is about 2/3 of the calculation in Ref. [16].

4.2 Variation characteristics along with bias angle

1) With the burial depth of the shallow-buried side fixed, the total vertical loads on the deep-buried and shallow-buried side increase with the bias angle, as shown in Fig. 9. The reason is that as the bias angle increases, the thickness of the overlying earth on top of the tunnel increases gradually. As a result, the pressure of loose surrounding rock acting on the tunnel after excavation increases as well.

2) The single tunnel on the deep-buried and shallow-buried side is analyzed. As the bias angle increases, the vertical load (i.e. q_1, q_3) on the shallow-buried side decreases gradually; while that (i.e. q_2, q_4) on the deep-buried side increases. This indicates the presence of unsymmetrical loading effect, which is more prominent on the shallow-buried side (left tunnel), as shown in Fig. 10. That is to say, the load on the shallow-buried side (deep-buried side) of left tunnel (shallow-buried side) decreases (increases) more significantly with the increasing bias angle, compared with the deep-buried side. This is because during the increase of the thickness of overlying earth with the increasing bias angle, the

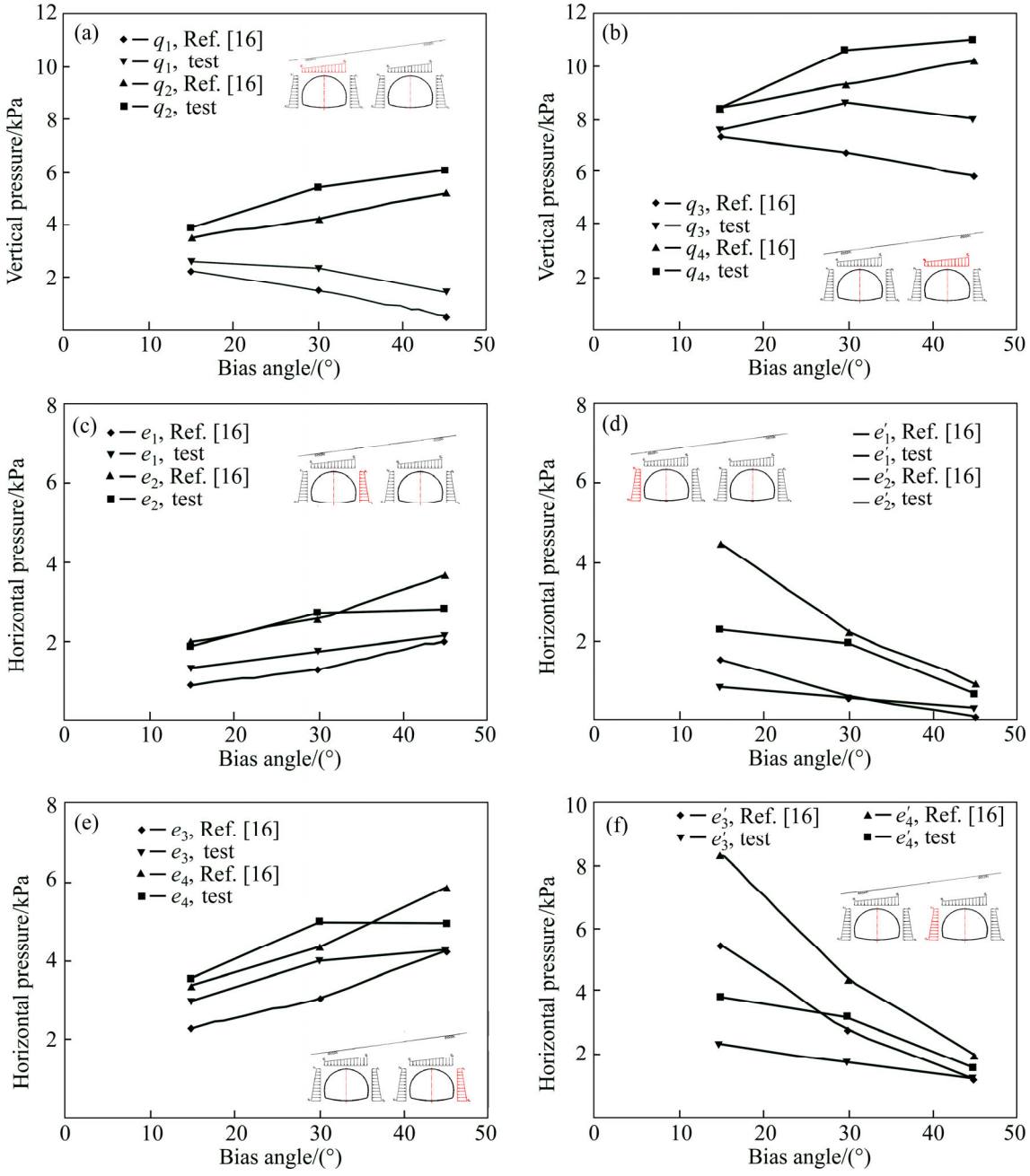

Fig. 10 Variation tendency of surrounding rock pressure with bias angle

loose surrounding rock pressure on the tunnel of the shallow-buried side increases. However, the right tunnel (deep-buried side) begins to conform to deep-buried conditions, and the surrounding rock shows the features of self-supporting capacity. So, the surrounding rock pressure stabilizes.

Thus, the method for estimating the load on the shallow-bias tunnels with small clear distance should be modified (see Fig. 11 and Eq. (1)).

$$\begin{Bmatrix} \boldsymbol{q}^{\mathrm{R}} \\ \boldsymbol{e}^{\mathrm{R}} \\ \boldsymbol{e}'^{\mathrm{R}} \end{Bmatrix} = \{\boldsymbol{q} \quad \boldsymbol{e} \quad \boldsymbol{e}'\} \begin{bmatrix} \boldsymbol{k}_q & & \\ & \boldsymbol{k}_e & \\ & & \boldsymbol{k}_{e'} \end{bmatrix} \tag{1}$$

where $\{\boldsymbol{q}^{\mathrm{R}}\ \boldsymbol{e}^{\mathrm{R}}\ \boldsymbol{e}'^{\mathrm{R}}\}^{\mathrm{T}}$ is the corrected surrounding rock pressure of shallow-bias tunnels with small clear distance; $\{\boldsymbol{q}\ \boldsymbol{e}\ \boldsymbol{e}'\}$ is the value calculated in Ref. [16]; $[\boldsymbol{K}]$ is the correction coefficient. Then, the expression is written as

$$\left\{\boldsymbol{q}^{\mathrm{R}} \quad \boldsymbol{e}^{\mathrm{R}} \quad \boldsymbol{e}'^{\mathrm{R}}\right\}^{\mathrm{T}} = \left\{\left\{q_i^{\mathrm{R}}\right\} \quad \left\{e_i^{\mathrm{R}}\right\} \quad \left\{e_i'^{\mathrm{R}}\right\}\right\}^{\mathrm{T}},\ i = 1,\ \cdots,\ 4;$$

$$\{\boldsymbol{q} \quad \boldsymbol{e} \quad \boldsymbol{e}'\} = \left\{\left\{q_i\right\} \quad \left\{e_i\right\} \quad \left\{e_i'\right\}\right\},\ i = 1,\ \cdots,\ 4;$$

$$[\boldsymbol{K}] = \begin{bmatrix} \boldsymbol{k}_q & & \\ & \boldsymbol{k}_e & \\ & & \boldsymbol{k}_{e'} \end{bmatrix} = \begin{bmatrix} \{k_{q_i}\} & & \\ & \{k_{e_i}\} & \\ & & \{k_{e_i'}\} \end{bmatrix}.$$

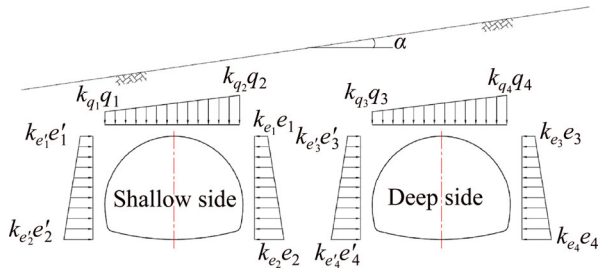

Fig. 11 Modified loading mode of shallow bias tunnels with small clear distance

The values of the correction coefficients are determined in Table 3 under the experimental working conditions.

Table 3 Correction factor of surrounding rock pressure under experimental conditions

Bias angle/(°)	k_{q_1}	k_{q_2}	k_{q_3}	k_{q_4}	k_{e_1}	k_{e_2}
15	1.2	1.1	1.0	1.0	1.5	1.0
30	1.6	1.3	1.3	1.1	1.4	1.1
45	3.0	1.2	1.4	1.1	1.0	0.8
Bias angle/(°)	k_{e_3}	k_{e_4}	$k_{e_1'}$	$k_{e_2'}$	$k_{e_3'}$	$k_{e_4'}$
15	1.3	1.0	0.5	0.5	0.4	0.5
30	1.3	1.2	1.0	0.9	0.6	0.7
45	1.0	0.8	3.6	0.7	1.1	0.8

5 Conclusion and suggestions

1) The failure development of surrounding rock of shallow-bias tunnels with small clear distance can be summarized as follows: deformation of tunnel and strata → formation of micro-fracture surfaces in the periphery of tunnel → fracture surfaces extending deep into the surrounding rock in a larger density → tensile cracking in shallow position on deep-buried side and shear slip in deep layer → rapid deformation and slip on shallow-buried side → collapse. The vulnerable sites of fracture are the periphery of the tunnel and the strata in the shallow position of the deep-buried side.

2) The failure mode of shallow-bias tunnels with small clear distance is featured by an inverted conical fracture with tunnel arch as top and the slope at tunnel entrance as bottom. The scope of fracture on the deep-buried side is significantly larger than that on the shallow-buried side. As the bias angle increases, the scope of fracture is enlarged. Compared with the "linear fracture surface" model, the fracture angles on the two sides of the proposed model are larger; the fracture angles on the two sides of the middle rock pillar are slightly smaller; and the bottom of the fracture is located on the springing line of tunnel arch.

We suggest that the surrounding rock mass on the deep-buried side should be reinforced apart from the tunnel surrounding rock for shallow-bias tunnels with small clear distance. Moreover, the scope of consolidation should go beyond the midline of tunnel by 4*D* (along the direction of the top of slope).

3) The total vertical loads on the deep-buried and shallow-buried sides increase with the increasing bias angle. Compared with the existing calculations, the load on the shallow-buried side (deep-buried side) in the left tunnel decreases (increases) more significantly with the increasing bias angle than on the deep-buried side. This indicates a more prominent unsymmetrical loading effect. Therefore, it is necessary to modify the load values of shallow-bias tunnels with small clear distance based on the existing calculations.

It should be noted that the measurement data only apply to the experimental working conditions. For situations other than the experimental working conditions, more engineering practices and theoretical efforts are needed.

References

[1] GONG Jian-wu, XIA Cai-chu, LEI Xue-wen. Analysis of filed measurement and theoretical calculation on rock pressure in shallow-buried twin tunnels with small spacing [J]. Chinese Journal of Rock Mechanics and Engineering, 2010, 29(Suppl. 2): 4139−4145. (in Chinese)

[2] YAMAGUCHI I, YAMAZAKI I, KIRITANI Y. Study of ground-tunnel interactions of four shield tunnels driven in close proximity, in relation to design and construction of parallel shield tunnels [J]. Tunnelling and Underground Space Technology, 1998, 13: 289−304.

[3] KOOI C B, VERRUIJT A. Interaction of circular holes in an infinite elastic medium [J]. Tunnelling and Underground Space Technology, 2001, 16: 59−62.

[4] FU Jin-yang, YANG Jun-sheng, YAN Li, ABBAS S M. An analytical solution for deforming twin-parallel tunnels in an elastic half plane [J]. International Journal for Numerical and Analytical Methods in Geomechanics, 2015, 39(5): 524−538.

[5] XIE Jun, LIU Chun-gui, YU Hai-yong. Upper bound solutions of plastic limit analysis for the stability of two parallel circular tunnels [J]. Chinese Journal of Rock Mechanics and Engineering, 2006, 25(9): 1835−1841. (in Chinese)

[6] SOLIMAN E, DUDDECK H, AHENS H. Two and three dimensional analysis of closely spaced double-tube tunnels [J]. Tunnelling and Underground Space Technology, 1993, 8(1): 13−18.

[7] GALLI G, GRIMALDI A, LEONARDI A. Three-dimensional modeling of tunnel excavation and lining[J]. Computers and Geotechnics, 2004, 31: 171−183.

[8] NG C W W, LEE K M, TANG D K W. Three-dimensional numerical investigations of new Austrian tunnelling method (NATM) twin tunnel interactions [J]. Canadian Geotechnical Journal, 2004, 41(3) : 523−529.

[9] CHU B L, HSU S C, CHANG Y L, LIN Y S. Mechanical behavior of a twin-tunnel in multi-layered formations [J]. Tunnelling and Underground Space Technology, 2007, 22: 351−362.

[10] CHAPMAN D N, AHN S K, HUNT D V L. Investigating ground movements caused by the construction of multiple tunnels in soft ground using laboratory model tests [J]. Canadian Geotechnical Journal, 2007, 44(6): 631−643.

[11] CHAPMAN, D N, AHN S K, HUNT D V L, CHAN A H C. The use of model tests to investigate the ground displacements associated with multiple tunnel construction in soil [J]. Tunnelling and Underground Space Technology, 2006, 21: 413−418.

[12] YANG Xiao-li, SUI Zhi-rong. Numerical simulation of construction sequence for shallow embedded bias tunnels with small clear distance [J]. Journal of Central South University: Science and Technology , 2007, 38(4): 764−770. (in Chinese)

[13] KARMEN F B, BORUT P. Displacement analysis of tunnel support in soft rock around a shallow highway tunnel at Golovec [J]. Engineering Geology, 2004, 75: 89−106.

[14] CHEN Jian-feng, KANG Chen-yang, SHI Zhen-ming. Displacement monitoring of parallel closely spaced highway shield tunnels in Marine clay [J]. Marine Georesources & Geotechnology, 2015, 33(1): 45−50.

[15] XIAO Ming-qing. Study on the rock pressure acting on shallow tunnels with small spacing [J]. Modern Tunnelling Technology, 2004, 41(3): 7−10. (in Chinese)

[16] SHU Zhi-le, LIU Bao-xian, LI Yue. Surrounding rock pressure analysis of neighbourhood tunnel under unsymmetrical pressure[J]. Chinese Journal of Underground Space and Engineering, 2007, 3(3): 430−433. (in Chinese)

[17] YANG Xiao-li, ZHANG Jia-hua, JIN Qi-yun, MA Jun-qiu. Analytical solution to rock pressure acting on three shallow tunnels subjected to unsymmetrical loads [J]. Journal of Central South University, 2013, 20(2): 528−535.

[18] ZHANG Hui, ZHANG Zi-xin, HUANG Hong-wei, DU Ju-hong. Model test on mechanical behavior of two shallow-buried closely-spaced tunnels at different elevations under unsymmetrical load [J]. Journal of Tongji University: Natural Science, 2009, 37(2): 169−175. (in Chinese)

[19] LEI Ming-feng, PENG Li-min, SHI Cheng-hua, WANG Li-chuan, LIU Zheng-chu. Model research on failure mechanism and lining stress characteristics of shallow buried tunnel under unsymmetrical pressure [J]. Journal of Central South University: Science and Technology, 2013, 44(8): 3316−3325. (in Chinese)

[20] LEI Ming-feng, PENG Li-min, SHI Cheng-hua. Model test to investigate the failure mechanisms and lining stress characteristics of shallow buried tunnels under unsymmetrical loading [J]. Tunnelling and Underground Space Technology, 2015, 46: 64−75.

(Edited by YANG Hua)